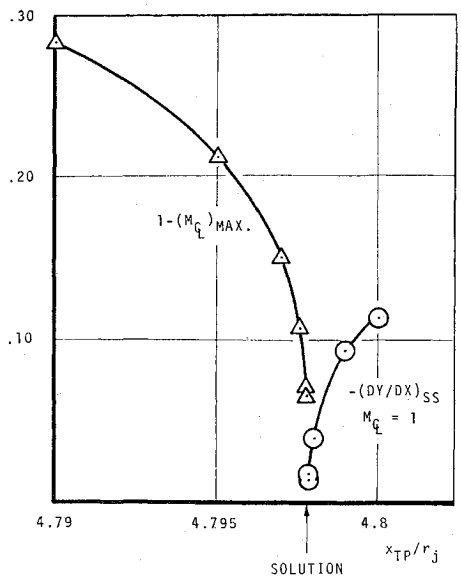

Fig. 4. Parameters pinpointing the solution.

As the computation proceeds downstream of the triple point, the solution for the subsonic streamtube will follow either an accelerating or a decelerating branch, depending on whether the assumed value of x_{TP} is too small or too large. Near the correct triple point abscissa neither case quickly prevails, and the current "branch" does not become evident until the pressure gradient actually begins to increase or decrease catastrophically (in the first case this is evident by the catastrophic increase in θ_{SS}).

For the case computed, the axial variation in core streamtube Mach number (Fig. 2) clearly shows the two branches, depending on whether the assumed value for x_{TP} is greater than or less than the solution. In particular, notice the "cusping" of the stagnating branch as x_{TP} approaches the solution.

One of the most revealing figures is a plot of $(dy/dx)_{SS}$ vs M_{ℓ} (Fig. 3). The saddle point behavior is quite evident, particularly in the tendency of $d\theta(M)/dM$ to become discontinuous at $\theta = 0$ as $M = 1$ is approached on the stagnating branch. Notice the convergent-divergent character of that branch when the figure is rotated 90° clockwise. It is clear from these two figures that, within the accuracy of these computations, this theory brackets x_{TP}/r_j between 4.79784 and 4.79788. This is in good agreement with the experimental result of Love et al.[3] which placed the Mach disc on the axis at $x/r_j = 4.8 - 4.9$.†

In closing, it is of interest to consider how close each iteration comes to passing through the "throat" for each assumed value of the triple point location. On the stagnating branch, the quantity $1 - (M_{\ell})_{max}$ measures closeness well, while on the accelerating branch, the value of the slip stream slope, $(dy/dx)_{SS}$, where $M_{\ell} = 1$ is appropriate. These two curves strikingly point to the value of x_{TP} (Fig. 4).

References

[1] Crocco, L., "One-Dimensional Treatment of Steady Gas Dynamics," *High Speed Aerodynamics and Jet Propulsion, Vol. III, Fundamentals of Gas Dynamics*, edited by H. W. Emmons, Princeton Univ., Princeton, N.J., 1958.

[2] Crocco, L., "Considerations on the Shock-Boundary Layer Interaction," *High Speed Aeronautics*, edited by A. Ferri, N. J. Hoff, and P. Libby, Polytechnic Institute of Brooklyn, 1955.

[3] Love, E. S. et al., "Experimental and Theoretical Studies of Axisymmetric Free Jets," R6, 1959, NACA.

† Note that Love[3] measured the Mach disk abscissa, which is slightly downstream of x_{TP}.

Forces on an Inclined Circular Cylinder in Supercritical Flow

W. J. Bootle*
Avco Systems Division, Wilmington, Mass.

Nomenclature

C_D = cylinder drag coefficient based on planform area
C_{D_c} = pressure drag of elliptic section normal to the flow
C_L = cylinder lift coefficient based on planform area
C_N = cylinder normal force coefficient based on planform area
C_f = friction coefficient based on wetted area
D = drag
N = normal force
Re = Reynolds number
S = planform area (dl)
S_e = frontal area of elliptic section ($dl \sin\alpha$)
V = flow velocity
c = major axis of elliptic section
d = cylinder diameter
h = height of elliptical section of an element of cylinder
l = length of an element of an infinite cylinder
q = dynamic pressure
t = minor axis of elliptic section
α = angle of attack
ν = kinematic viscosity

Subscripts

∞ = based on freestream conditions
c = based on cross flow conditions
turb = turbulent flow conditions

THE classical method for estimating the aerodynamic forces acting on an inclined circular cylinder in low-speed flow is based on the cross-flow principle wherein the flow component normal to the body is treated as independent of that along it. In terms of freestream dynamic pressure and planform area, the normal force coefficient then becomes $C_{D_c} \sin^2\alpha$, where C_{D_c} is the section drag coefficient for the unyawed cylinder, and the axial force component due to friction becomes $\pi C_f \cos^2\alpha$; in turn the following expressions are obtained for C_L and C_D:

$$C_L = C_{D_c} \sin^2\alpha \cos\alpha - \pi C_f \cos^2\alpha \sin\alpha \quad (1)$$

$$C_D = C_{D_c} \sin^3\alpha + \pi C_f \cos^3\alpha \quad (2)$$

The method is known to give good correlation with test data in sub-critical flow, but to fail[1,2] in supercritical flow at cross flow Mach numbers below 0.5. During transition there is a reduction in C_{D_c} which for smooth cylinders ranges from a sub-

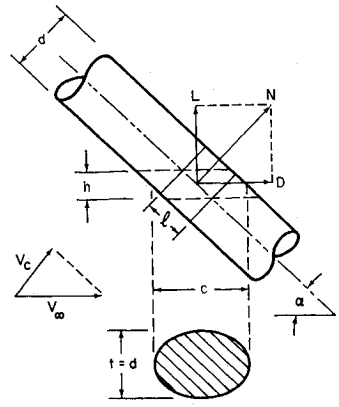

Fig. 1 Schematic representation of the analytical model.

Received March 5, 1970; revision received October 26, 1970. The author wishes to express his appreciation to E. E. H. Schurmann, Chief, Aerodynamics Section, Engineering Directorate, for his helpful suggestions during a review of the paper.

* Group Leader, Vehicle Dynamics, Flight Mechanics Section, Engineering Directorate. Member AIAA.

critical value of 1.2 to about 0.25 supercritical. The critical Reynolds number based on cross flow is strongly dependent on the angle of yaw,[2] ranging from 3.5×10^5 at zero yaw to about 1.0×10^5 at 60°. However, when based on stream flow it remains essentially constant at the unyawed value. As the cylinder is yawed, the value of C_{D_c} does not stay constant as in laminar flow, but increases with the yaw angle, while the equations for C_L and C_D are found to be in error even when allowance is made for the change in C_{D_c}. These trends suggest that the turbulent boundary layer prevents the axial and cross flows from acting independently; the interaction modifies the pressure distribution and the pressure drag. The object of this Note is to offer a semiempirical method for estimating supercritical force coefficients at low cross Mach numbers consistent with the observed behavior.

Consider an element l of an infinite circular cylinder inclined at an angle of attack α to the flow (Fig. 1). Assume that in turbulent flow the boundary layer exhibits negligible cross flow with respect to the inviscid streamlines. These streamlines approach the contour of the elliptic sections cut by planes containing the freestream velocity vector. The force N normal to the cylinder must then have a drag component D whose value is the same as that of the elliptic section in two-dimensional flow. Thus, $C_N q_\infty S \sin\alpha = C_{D_e} q_\infty S_e$ from which

$$C_N = C_{D_e} \tag{3}$$

The corresponding lift and drag coefficients then are

$$C_L = C_{D_e} \cos\alpha \tag{4}$$

$$C_D = C_{D_e} \sin\alpha \tag{5}$$

and, if the cross flow dynamic pressure is used for reference, the normal force coefficient from Eq. (3) becomes:

$$C_{N_c} = C_{D_e} \csc^2\alpha \tag{6}$$

Now consider C_{D_e}. In fully turbulent flow the pressure drag of elliptic sections is given by the empirical expression[3]

$$C_{D_e} = 120 C_{f_{turb}} (t/c)^2 \tag{7}$$

where t has the same meaning as d here. Equation (7) is valid for c/t above 1.6 in the case of smooth sections; a correction must be made as the section becomes circular, otherwise C_{D_e}

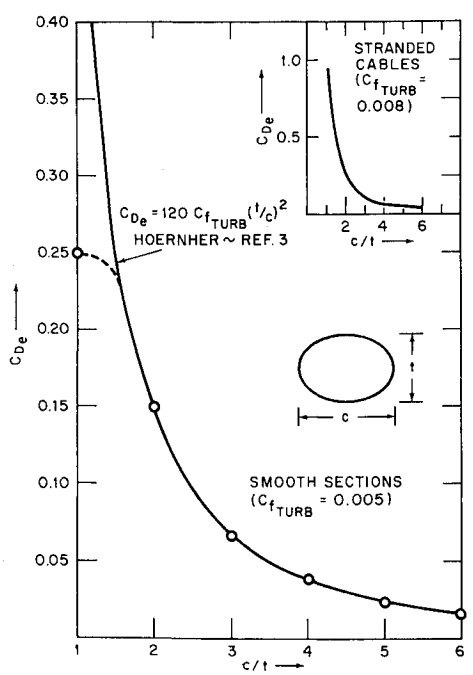

Fig. 2 Pressure drag of elliptic cylinders in supercritical flow as a function of chord/thickness ratio.

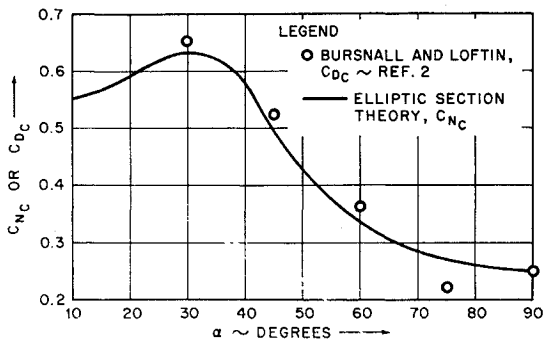

Fig. 3 Comparison of theoretical and experimental values for cross-flow force coefficient as a function of angle of attack.

is too high when compared with measured values. A curve based on Eq. (7) is presented in Fig. 2 together with the appropriate correction. The inset shows a corresponding curve for cables which will be discussed later. Thus, for $c/t \geq 1.6$, i.e., for sweep angles $\geq 50°$, one can substitute for C_{D_e} from Eq. (7) into the preceding equations to obtain

$$C_N = 120 C_{f_{turb}} \sin^2\alpha \tag{8}$$

$$C_L = 120 C_{f_{turb}} \sin^2\alpha \cos\alpha \tag{9}$$

$$C_D = 120 C_{f_{turb}} \sin^3\alpha \tag{10}$$

$$C_{N_c} = 120 C_{f_{turb}} \tag{11}$$

which are similar in form to those in crossflow theory, except that C_{D_c} is replaced by the variable term $C_{N_c} = 120 C_{f_{turb}}$. When the normal component of skin friction acting in the stream direction is included, the total cross flow force coefficient becomes

$$C_{N_{c_{total}}} = 120 C_{f_{turb}} + \frac{\pi C_{f_{turb}}}{\sin\alpha} \tag{12}$$

where it is implied that $C_{f_{turb}}$ is based on the streamwise Reynolds number $V_\infty c/\nu$. At smaller sweep angles ($\alpha \geq 40°$) where Eq. (7) overpredicts C_{D_e}, one must replace the term $120\, C_{f_{turb}}$ in Eq. (12) by Eq. (6) with C_{D_e} taken from the corrected curve of Fig. 2.

Comparison with Test Data

Test data are available[2] for the cross force coefficient of a smooth cylinder in turbulent flow at yaw angles up to 60°. To effect a comparison, Eq. (12) has been solved using a friction coefficient at a streamwise Reynolds number commensurate with the cross Reynolds numbers quoted in the reference. Comparative results are shown in Fig. 3. It is seen that excellent agreement is obtained.

Data are also available for stranded cables. These show a terminal value for $C_{f_{turb}}$ of about 0.008 for $Re \geq 10^4$ because surface imperfections produce turbulent flow. If this value of $C_{f_{turb}}$ is used in Eq. 12, then C_{N_c} at normal incidence is 0.985, very close to the practical value of 1.0.[3] Thus, Eq. (7) can be applied to cables without restriction (see the inset curve in Fig. 2).

If the normal force acting on a cable element of length l is evaluated by means of Eq. (12) it is seen that

$$N = q_\infty \sin^2\alpha (dl) [120 C_{f_{turb}} + \pi C_{f_{turb}}/\sin\alpha]$$
$$\text{i.e., } N/\sin^2\alpha = A + B/\sin\alpha \tag{13}$$

where A and B are constants at a fixed value of q_∞. This result is in direct agreement with an empirical rule developed by the David Taylor Model Basin which is known to apply for cross-flow Reynolds numbers up to 2×10^5.

References

[1] Allen, H. J., "Estimation of the Forces and Moments Acting on Inclined Bodies of Revolution of High Fineness Ratio," RM A9126, Nov. 1949, NACA.

[2] Bursnall, J. and Loftin, K., "Experimental Investigation of the Pressure Distribution About a Yawed Circular Cylinder in the Critical Reynolds Number Range," TN 2463, Sept. 1951, NACA.

[3] Hoernher, S. F., *Fluid Dynamic Drag*, 1965 edition, published by the author, 148 Busteed Drive, Midland Park, N.J., 07432, pp. 3–11, 4–5, 5–3, 6–2, 3.

Artificial Simulation of Micrometeoroids

SIEGFRIED AUER*

Deutsche Forschungs- und Versuchsanstalt für Luft- und Raumfahrt, Bad Godesberg, Germany

Facilities

WE possess powerful machines which are able to accelerate projectiles to meteoric velocities. The well-known light gas gun can shoot projectiles of centimeter size at velocities up to10 km/sec. Further, there is the electrostatic accelerator with an upper limit in velocity for micron-sized particles of about 70 km/sec, and the linear accelerator which, at a length of 1 km, could in principal bring a particle of 1 μ radius to a velocity of 1000 km/sec. Several circular and magnetic techniques are under discussion, as well as the laser powered accelerator which causes rocket-like propulsion by asymmetric evaporation of the particle. Finally there is the technique that uses the momentum flux of an electron beam to push a negatively charged particle forward.

Some people hope to initiate fusion reactions with the projectiles from such machines and to observe the Lorentz contraction. However, the existing facilities are rather limited. Even a velocity exceeding the escape velocity of the Earth, 11 km/sec, is difficult to achieve for a particle with a radius of 1 μ. Beyond that, a strict selection of projectile material is necessary, and additionally, the density of the projectiles must be as high as possible.

Most of the experiments described here were carried out with iron microspheres from electrostatic dust accelerators

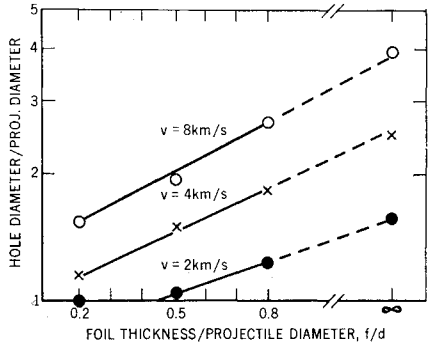

Fig. 1 Hole diameter as a function of foil thickness.

Presented as Paper 70-30 at the AIAA 8th Aerospace Sciences Meeting, New York, January 19–21, 1970; submitted April 31, 1970; revision received July 14, 1970.

* Member of German Helios Project Office.

at 0.1–3 million v. The radii of the projectiles were usually of the order of 1 μ, the velocities ranging from 0.5 to 40 km/sec. A critical velocity was observed at 4 to 6 km/sec. Below 4 km/sec the impact is nonexplosive. Above 6 km/sec the impact is always explosive, and no principal difference is observed at velocities between 6 and 40 km/sec. We will mainly discuss the velocity range above 4-6 km/sec because it includes most of the meteoric velocities. Furthermore, no fundamental difference in the behaviour of different materials has been found. Therefore, we can expect that our conclusions have some general validity in spite of the restrictions which are imposed by the existing facilities.

Meteor Studies

When a meteoroid enters the atmosphere of the Earth, collisions with gas molecules cause it to radiate and to leave a trail of ions behind itself. In order to simulate the processes, Friichtenicht et al.[1] injected iron microparticles with velocities between 15 and 45 km/sec into an air target. They measured the total radiant energy in the spectral band 3400–6300 Å and found that it was nearly independent of velocity in the range 20 to 40 km/sec, namely about 0.5% of the kinetic energy of the projectile.

Further, this group[2] measured the number of ions produced by the total ablation of projectiles in air. They found that at a velocity between 20 and 45 km/sec, about 6 and 80%, respectively, of the total number of atoms of the projectile were ionized. In an argon target the ionization was a factor of 2–4 lower.

Crater Studies

A micrometeoroid produces a crater at impact on a solid material, and the process differs completely from that of a contaminating particle which sinks slowly on the same surface. The intention of a collection experiment is to determine mass, velocity, composition and number of micrometeoroids. To achieve this, a series of investigations has been accomplished with the Heidelberg dust accelerator using iron projectiles for micrometeoroid simulation.

The crater shape was studied by Rudolph[3] with an electron stereoscan. This instrument uses the secondary electron yield of the sample surface, which is a strong function of the angle of inclination, to get a stereoscopic image of the surface roughness. In the particular case of a crater, its diameter, depth, general shape, surface roughness and the width of its rim can be determined.

Rudolph found that the crater volume is proportional to the kinetic energy of the projectile. He demonstrated quantitatively the following to be valid: The amount of energy which would be necessary to heat and melt the material which has been in the crater before its formation is equal to the kinetic energy of the projectile. This explains why, under equal conditions, a crater in lead is more than a factor of 10 larger in volume than a crater in beryllium.

Further, he found that the shape of a crater is typical for each target material. In particular the ratio depth-to-diameter T/D is constant for a projectile velocity in excess of 4 km/sec. Craters are semispherical, approximately, with T/D equal to about 0.5 in most of the target materials investigated, namely Ag, Au, Cd, Ni, Pb, Pd, Ta and Ti, and cylindrical with T/D equal to 1.0 in Al and Be targets. At a velocity below 4 km/sec, the crater shape is changing with velocity. Between 0.5 and 1.0 km/sec the projectile sticks nearly unchanged in the target. The crater diameter D is equal to the projectile diameter d, while the crater depth T is increasing rapidly with velocity. Above 1.0 km/sec up to approximately 4 km/sec, the crater diameter D is increasing more rapidly with increasing velocity than the crater depth T. Thus, from the ratio T/D and from the condition of the projectile which is found in the crater, one can directly estimate the projectile velocity. Above 4 km/sec, diameter